Plasticity Induced by Shock Waves in Nonequilibrium Molecular-Dynamics Simulations

Brad Lee Holian* and Peter S. Lomdahl

Nonequilibrium molecular-dynamics simulations of shock waves in three-dimensional 10-million atom face-centered cubic crystals with cross-sectional dimensions of 100 by 100 unit cells show that the system slips along all of the available {111} slip planes, in different places along the nonplanar shock front. Comparison of these simulations with earlier ones on a smaller scale not only eliminates the possibility that the observed slippage is an artifact of transverse periodic boundary conditions, but also reveals the richness of the nanostructure left behind. By introducing a piston face that is no longer perfectly flat, mimicking a line or surface inhomogeneity in the unshocked material, it is shown that for weaker shock waves (below the perfect-crystal yield strength), stacking faults can be nucleated by preexisting extended defects.

Almost 20 years ago, nonequilibrium molecular dynamics (NEMD) simulations, where Newton's equations of motion are solved on the computer for thousands of strongly interacting atoms, were first used to study true shock waves at the atomistic level (*1–4*). True shock waves exhibit steady profiles (density, velocity, stress, and energy), which accompany dissipative, irreversible flow of atoms in the directions transverse to the planar wave propagation. NEMD simulations demonstrated that the method is particularly ideal for dense-fluid shock waves, where thicknesses are only a few molecular spacings, rise times are only a few collision times, and viscous flow in the shock front leads to steady waves (*3*). Subsequently, Hoover showed that a continuum constitutive model, using the Navier-Stokes equations of hydrodynamics, could explain the observed NEMD profiles (*5*). Further NEMD simulations for even stronger fluid shock waves, where the shock thickness corresponds to only two or three molecular spacings, showed that the Navier-Stokes equations are nevertheless still valid (*4*).

Whereas viscous flow in dense-fluid shock waves is highly localized, shock propagation in solids is inherently more complex, because solids introduce a new length scale other than the lattice spacing, namely, the size of defects that govern plastic flow. In general, plastic deformation in solids results from the creation and motion of dislocations (a dislocation is a lattice mismatch along a slip plane and is characterized by long-range stress and strain fields). In the early 1980s, shock-wave structure in solids was elucidated at Los Alamos National Laboratory in NEMD simulations by Holian, Straub, and Swanson (*1, 2, 6, 7*). These calculations showed that planar shock waves in single crystals became steady waves through transverse displacements of atoms, not by viscous flow as in fluid shock waves (*3–5*), but rather by plastic flow, that is, concerted slippage of atoms over each other. In the Lennard-Jones (LJ) pair-potential solid, represented by the face-centered cubic (fcc) lattice, a shock wave traveling in the ⟨100⟩ direction results in slippage along one of the four available {111} planes, by emission at the shock front of a Shockley partial dislocation, which leaves behind a stacking fault (the usual ABCABC . . . stacking of triangular-lattice close-packed planes becomes ABABCA . . .).

In order to minimize edge effects and thereby model an infinite plate of material, NEMD shock-wave simulations have traditionally used periodic boundary conditions transverse to the shock-wave propagation direction. NEMD calculations done as recently as a decade ago (*6*) were severely limited in the length of run in the direction of shock-wave propagation needed to achieve a steady wave and in the transverse cross-sectional area. A typical simulation might be on the order of 100 lattice planes in length along the shock propagation direction, and approaching 100 atoms in each cross-sectional plane, or 10,000 atoms total in three dimensions (3D). Computational times are then limited by the sound-traversal time in the shock-propagation direction, on the order of 25 vibrational periods (~5 ps). Shock thicknesses are then restricted to be less than ~10 nm, with rise times of the order of a picosecond. Thus, weak shock waves, whose thicknesses are measured in fractions of micrometers with presumably similar sizes of cross-sectional structures, are well beyond the reach of atomistic simulations.

In spite of these computational limitations in time and space, it is remarkable that solid shock waves—if they are not too weak—are nevertheless amenable to NEMD simulations. It is especially noteworthy that the rich details of shock-wave structure are hardly visible in the set of shock velocities u_s obtained in simulations of various strengths or piston velocities u_p (Fig. 1). This so-called Hugoniot relation is a global statement of mass, momentum, and energy conservation linking a given initial equilibrium state to all possible final equilibrium states for steady planar shock waves, depending on their strength. It says nothing at all about the structure of the shock front, nor anything about dissipative structural rearrangement mechanisms that could lead to a steady shock wave.

For more localized detail in the shock front region, we can easily obtain shock-wave profiles from NEMD simulations, such as pressure-volume ($\boldsymbol{P}V$) tensor components, normal and transverse to the propagation direction, and the shear stress τ (one-half the difference between the normal and transverse components of $\boldsymbol{P}$). Shock-wave profiles from earlier simulations (*6*) in perfect crystals showed that once a steady state has been achieved, τ builds up to a maximum value τ_{max} at the

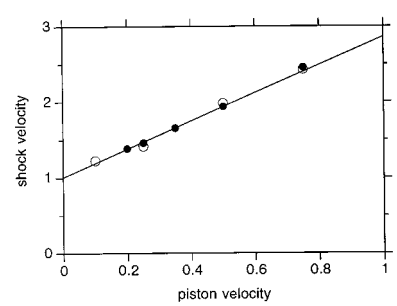

Fig. 1. Shock velocity (u_s/c_0) versus piston velocity (u_p/c_0) for atoms in 3D fcc solid (⟨100⟩ propagation direction) interacting via $\phi(r)$, the intermediate-range LJ spline pair potential (*13, 14*). Initial density is $\rho_0 = \sqrt{2}m/r_0^3$, where m is atomic mass, r_0 is nearest neighbor distance ($a_0 = \sqrt{2}r_0$ is initial fcc lattice constant), ε_0 is bond energy, and c_0 is 1D longitudinal sound speed, such that $mc_0^2 = 72\varepsilon_0 = r_0^2\phi''(r_0)$. Initial temperature is $kT/\varepsilon_0 = 0.001$. L is cross-sectional periodic boundary length; the open circles are previous simulations for $L/a_0 = 6$ unit cells (*6*); solid circles are the present simulations for $L/a_0 = 100$, which have been fitted by straight line $u_s = c + su_p$, where $c = 1.01c_0$ and $s = 1.86$. Note that melting occurs near $u_p/c_0 \approx 1$ (*6, 19*).

Theoretical Division, Los Alamos National Laboratory, Los Alamos, NM 87545, USA.

*To whom correspondence should be addressed. E-mail: blh@lanl.gov

center of the shock front and is then relieved by transverse plastic flow. However, due to the limitation of small computational cross sections, these early profiles were very noisy. Our present simulations are for much larger systems and therefore exhibit much smoother profiles (Fig. 2). For shock strengths at and above a threshold limit, the ratio of the Hugoniot jump stress P to τ_{max} appears always to be $P/\tau_{max} \sim 10$ in 3D (*6*) (although our present large-scale simulations show that this ratio increases slowly with shock strength). At the threshold of shock-induced plasticity in perfect crystals, as observed in NEMD simulations, the critical value of $P \approx G$, where G is the shear modulus, so that $\tau_{max} \approx G/10$, roughly the ideal-crystal yield strength. Provided that we could unambiguously rule out the effect of transverse periodic boundary conditions, we speculated (*6*, *7*) that preexisting defects such as vacancies, dislocations, or grain boundaries might considerably lower this ideal crystal threshold.

Pictures of atomic positions from our early NEMD simulations for shocks in perfect crystals revealed slippage beginning at the shock front, in the form of what appeared to be bands of stacking faults, though the spacing of the bands was clearly dictated by the transverse periodic boundaries. In fact, only a single slip system was randomly selected by thermal fluctuations, so that in principle, the results were consistent with the formation of a single stacking fault. For a stronger shock, two parallel stacking faults were seen (*6*). Long after our earliest NEMD results, experimental verification was obtained by Russian investigators, using dynamic shock-wave x-ray measurements of shifts in fcc-crystal diffraction peaks (*8*). [At the same time, we were doing dynamic shock-wave simulations at Los Alamos, Mogilevsky in the U.S.S.R. (*9*) was doing quasi-static relaxation simulations in uniaxially stressed fcc crystals and observing dislocation-emission events similar to those we saw; because of poor contacts between U.S. and Soviet scientists during the height of the Cold War, both sides were unaware of the others' work for several years.]

In the early 1990s, at Los Alamos (*7*), we simulated shock waves in 2D solids, where the cross-sectional area could be taken to be nearly an order of magnitude larger than previous 3D simulations. We observed that two of the three available triangular-lattice slip systems were activated, and the shock front became irregular, rather than perfectly planar as in the early purely elastic phase of propagation (*7*). It remained to be seen, however, whether these 2D observations would hold for large 3D systems, where the complexity of dislocation emission is considerably enhanced (*10*).

Here, we will explore the question of NEMD system size in evaluating observations of shock-wave–induced plasticity. Recent advances in computer technology, primarily massively parallel machines and the molecular-dynamics code we have developed (*11*), enabled us to simulate the atomistic behavior of 3D solid materials exposed to moderately strong shock waves for much larger systems (10^7 to 10^8 atoms) than were possible just a decade ago.

In NEMD simulations, there are three principal ways to generate a shock wave: (i) As in laboratory planar shock-wave experiments, one can computationally hurl a flyer plate toward a stationary target at a velocity of $2u_p$. This is equivalent to slamming the two plates against each other at $\pm u_p$; in this symmetric-impact case, a pair of shock waves moves out from the interface at $\pm u_s$. (ii) The symmetric impact can be generated by inhomogeneously shrinking the longitudinal periodic length. This is useful, particularly for fluid shock-wave simulations, for eliminating the effect of free surfaces (*4*). (iii) Material can be pushed by an infinitely massive piston moving at velocity u_p; all particles coming in contact with the piston face are specularly reflected by a flat momentum mirror. Equivalently, the piston can be at rest, with the unshocked target material given an initial velocity of $-u_p$; the shock wave then moves out from the stationary piston face at velocity $u_s - u_p$. We have found that, although there are some minor differences between these three shock-generation approaches, the first and third are most suitable for studying both shock-wave and release-wave phenomena in solids.

Preliminary calculations, which were 15 by 15 fcc unit cells in cross-sectional area, demonstrated that instead of a single-slip system being triggered by the shock wave,

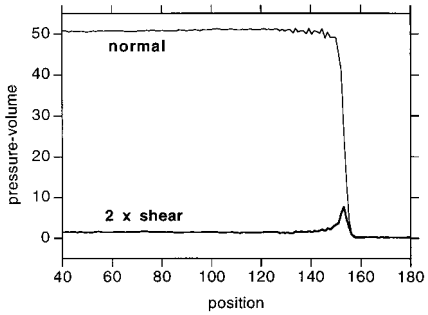

Fig. 2. Steady shock-wave profile (position/r_0) of pressure-volume tensor ($\boldsymbol{P}V/N\varepsilon_0$) components: normal to shock plane, and difference between normal and transverse (that is, 2 × shear), at piston velocity $u_p/c_0 = 0.5$ for square cross-sectional dimension of $L/a_0 = 100$ unit cells (20,000 atoms in cross-sectional planes).

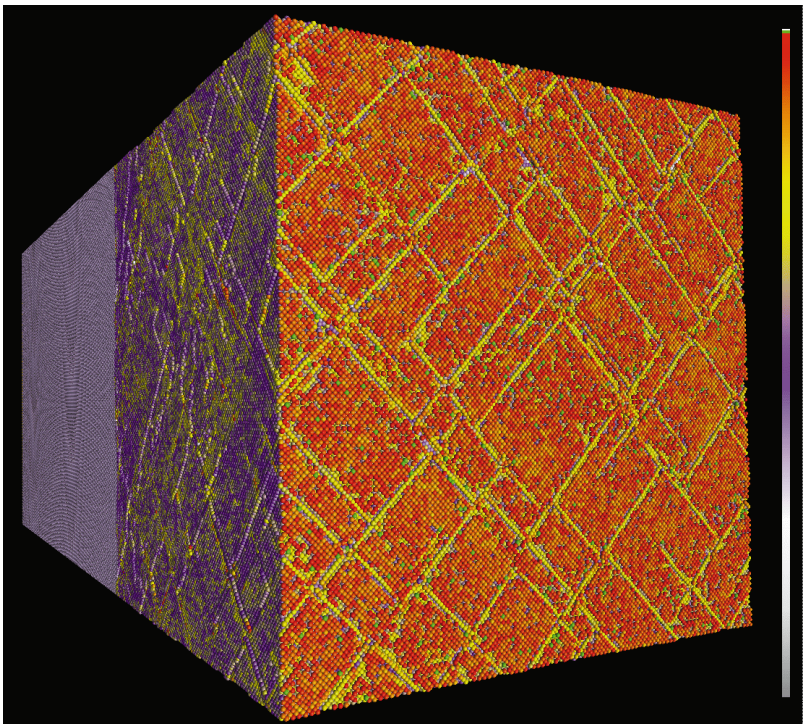

Fig. 3. Pattern of intersecting stacking faults at piston face (impact plane) induced by collision with momentum mirror at piston velocity $u_p/c_0 = 0.2$ for square cross-sectional dimension of $L/a_0 = 100$ unit cells; shock wave has advanced halfway to the rear (~250 planes). Atoms are colored according to potential energy (see color bar at side, energy increasing from bottom).

slippage occurred along two different {111}-type planes. This behavior is reminiscent of the idealized model of C. S. Smith (*12*), where the shock front in a perfect lattice creates pairs of dislocations that accommodate the increased density of the shocked material, leaving the crystal orientation virtually unchanged, at the same time that the shear stress is relieved. However, the dynamic results are richer than this static picture: the slippages on the two systems compete with each other, causing the front to become somewhat unstable, with the leading slip system making the front bulge out ahead by two or three lattice spacings (as in the 2D case). These slipped regions are clearly stacking faults, as can be seen by looking at the oncoming shock front along the shock-propagation direction. It appears that the interaction potential does not affect this shock-induced slippage so much as the geometry of the fcc crystal structure itself; both LJ pair-potential and embedded-atom-method (EAM) many-body potential materials [such as copper (*10, 13, 14*)] exhibit this behavior. Consistent with the easier generation of dislocations, however, the EAM system has a lower threshold shock strength for plastic flow (*14*).

We tested the hypothesis that preexisting point defects could trigger plastic deformation by first placing a single vacancy, and then a di-vacancy, in the path of a shock wave, whose strength had been insufficient to initiate plastic flow in the small cross-section perfect crystal. No plastic deformation was triggered by either of these defects, though there was considerable acoustic disturbance in the front as the wave passed over them. This is in contrast to shock waves in 2D lattices, where vacancies are analogous to line defects in 3D, and therefore appear to be more effective in triggering plastic flow (*15*).

We found that the critical transition in shock strength between elastic and plastic behavior is essentially independent of the initial temperature T_0 [provided that T_0 is not equal to zero, where plasticity appears to be artificially prohibited, regardless of shock strength (*1*)]. We varied the initial temperature all the way from half the melting temperature T_M down to $0.001T_M$, with no visible effect on the sudden onset of plasticity with shock strength.

By expanding the cross-sectional area to 100 by 100 fcc unit cells in a 10-million-atom simulation, we are now able to answer definitively whether the sudden onset of plasticity observed in NEMD shock waves is real or an artifact of transverse periodic boundaries. With 4 by 4, 6 by 6, 10 by 10, or 15 by 15 cross sections, we were able to observe at most two stacking faults in the region of the transition ($u_p/c_0 \approx 0.2$); now, with 100 by 100, we are able to see that the shock wave propagates about 60 lattice planes, followed by the relatively sudden creation of a large number of stacking faults. These are distributed randomly on all four {111} slip systems and propagate back through the shocked, unslipped material, at a speed that is comparable to the sound speed in the compressed material, as well as forward with the shock front. As the shock wave propagates further, the front becomes pronouncedly nonplanar, with the front bulging by as much as 10 lattice planes. When viewed at an arbitrary {100} plane, the intersections emerge as a randomly spaced plaid pattern (Fig. 3). This demonstrates conclusively that we are no longer limited by periodic boundaries, but are seeing the true nature of plastic flow, at least in this intermediate regime of shock strength.

When we reduced the shock strength u_p/c_0 from 0.20 to 0.18, we saw that the plasticity drops sharply to zero. A rough dimensionless measure of plasticity is given by $a_0/\langle\ell\rangle$, where $\langle\ell\rangle$ is the average spacing between stacking faults. Above the sudden onset of shock-wave–induced plasticity, $a_0/\langle\ell\rangle$ follows closely the total volumetric strain u_p/u_s across the shock front (Fig. 4). The dramatic threshold in plasticity for the 100 by 100 system, just as in the smaller cross-section systems, is clearly due to an onset of ideal crystal yielding, rather than to periodic boundaries—that is, system size. We confirm this quantitatively by noting that, at the critical strength where shock-induced plasticity commences, the maximum nonhydrostatic (shear) pressure times half the volume change across the shock is almost exactly equal to the potential barrier to partial dislocation emission (the unstable stacking fault energy at constant volume), which is $0.16\varepsilon_0$ for the Lennard-Jones spline potential.

When the shock wave reaches the free surface and a rarefaction (relief) wave is produced, the stacking faults that were produced by shock compression are mostly an-

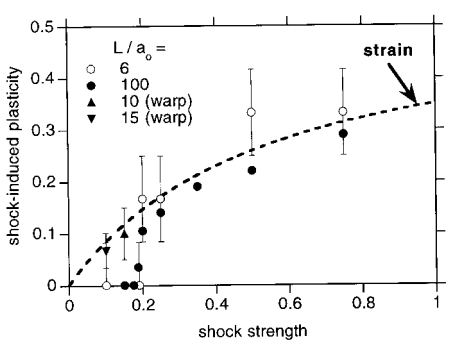

Fig. 4. Shock wave–induced plasticity $a_0/\langle\ell\rangle$ versus shock strength u_p/c_0 as function of cross-sectional periodic length L/a_0 (a_0 is the initial fcc lattice constant). Shock waves have been initiated in fcc-lattice ⟨100⟩-direction by flat momentum mirror at piston face, except as denoted by "warp," where warped momentum mirror with wavelength L and amplitude $h = r_0$ is positioned at $x(y) = h\cos(2\pi y/L)$. Resolution in measured plasticity is given by error bars, which are smaller than symbol size for $L/a_0 = 100$; total volumetric strain u_p/u_s across shock front is shown as heavy dashed curve.

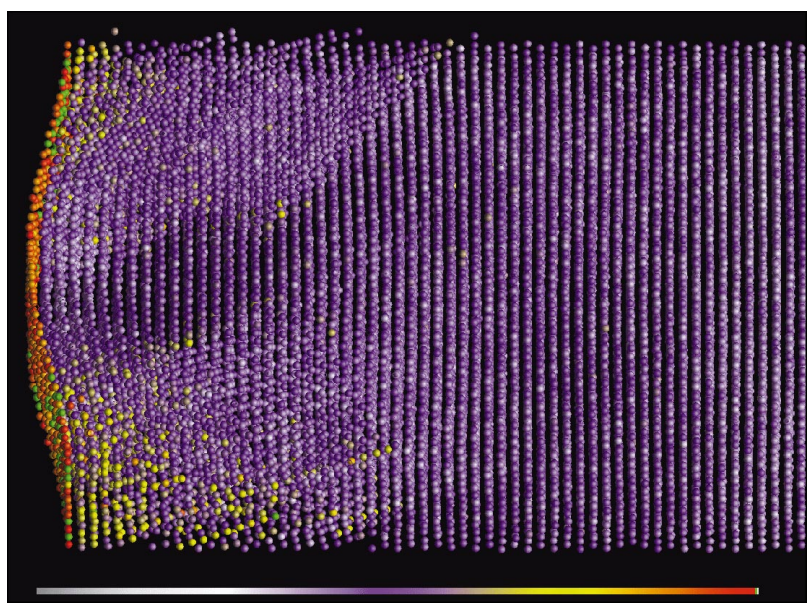

Fig. 5. Stacking faults initiated by collision with warped momentum mirror at piston velocity $u_p/c_0 = 0.1$ for square cross-sectional dimension of $L/a_0 = 15$ unit cells; shock wave has already advanced beyond window frame at right. Atoms are colored according to potential energy (see color bar at bottom, energy increasing from left); periodic box has been tilted around axis of shock propagation direction (left-to-right) by about 30 degrees to show stacking faults.

nihilated, at least for the 15 by 15 system, where only one or two slip systems are activated. This is consistent with the observation of much smaller dislocation densities in recovered shocked materials (*16*).

We tested the hypothesis that preexisting extended defects could trigger plastic deformation, by replacing the perfectly flat momentum mirror at the piston face by a warped mirror. That is, we introduced into the mirror a wave of amplitude h and wavelength L (the transverse periodic dimension), which, with only two arbitrary parameters, had the effect of mimicking a nonplanar impact surface, or of subjecting the shock front to a preexisting extended defect, such as a large inclusion, a dislocation, a stacking fault, or a grain boundary. We chose first the case $L = 10a_0$ and $h = r_0$ for a shock strength of $u_p/c_0 = 0.15$, where no plastic flow had previously been observed (at least for shocks initiated at a flat, mirror-smooth piston face in perfect crystals, even for $L = 100a_0$). With the warped mirror, we observed the production of stacking faults after the shock wave had traveled on the order of 50 lattice planes. This suggests that extended line or surface defects will probably trigger plastic flow when a planar shock wave passes over them.

At an even lower shock strength, namely $u_p/c_0 = 0.1$, and for $L = 15a_0$, we again observed the production of stacking faults (Fig. 5), although it was delayed by almost twice as long a propagation distance from the mirror (~100 planes). These warped-mirror results, mimicking interaction with preexisting extended defects, continue the trend of shock-induced plasticity proportional to volumetric strain that was seen above the onset perfect-crystal yielding (Fig. 4). The mode of plasticity is the same,

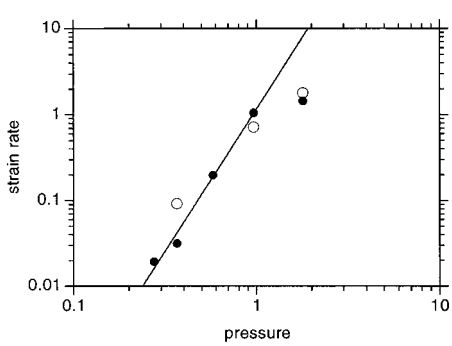

Fig. 6. Strain rate u_p/λ (in units of t_0^{-1}) versus shock pressure P (in units of $\rho_0 c_0^2$) as function of cross-sectional periodic length L; open circles are previous simulations for $L/a_0 = 6$ unit cells; solid circles are present simulations for $L/a_0 = 100$, with power-law fit for weaker shock strengths shown as straight line (slope = 3.3). u_p is piston velocity, λ is shock thickness, ρ_0 is initial density, c_0 is 1D longitudinal sound speed, and $t_0 = r_0(m/\varepsilon_0)^{1/2}$.

namely, the production of stacking faults by emission of partial dislocations near the shock front; however, the mechanism of nucleation has changed from heterogeneous at low strengths, requiring the help of preexisting extended defects, to homogeneous nucleation, or intrinsic plasticity due to perfect-crystal yielding at higher strengths.

A measure of the shock thickness λ is provided by the volumetric strain rate $\dot{\varepsilon} = u_p/\lambda$ as a function of the pressure rise P across the shock wave (Fig. 6). The shock thickness is measured from the shear-stress profile of the steady wave by reading off the exponential decay length (back to zero stress), beginning at the peak value; this is equivalent to constructing a maximal-slope tangent line at the middle of the shock front for the normal-stress profile, and reading off the difference between the intercepts for the maximum and minimum stress asymptotes (Fig. 2). The strongest shock appears to reach an asymptotic strain rate; therefore, we fitted the weaker shock waves to a power law of the form $\dot{\varepsilon} \sim P^m$, where $m = 3.3$. For real metals, where the shock strengths were much lower than what we have so far been able to achieve with NEMD (*17*), the experimental range for m is between 3 and 4.

Thus, it appears more and more likely that these new large-scale NEMD simulations, with the inclusion of realistic inhomogeneities, will be able to bridge the time and length scales to macroscopic experiments and provide essential input to continuum constitutive models. This conclusion has far-reaching implications beyond understanding shock-induced plasticity; for example, large-scale NEMD can be applied to defect-controlled aspects of shock-induced chemistry and detonations (*18*).

Issues remaining to be resolved include, first of all, the development of a more detailed structural model of partial dislocations, both in their creation under compressive shock-wave loading and in their annihilation upon relief-wave unloading from free surfaces. Both processes will require further atomistic studies, using systems with large cross sections. Second, while it is well known (*14*) that the slope of the Hugoniot curve (Fig. 1) is related to the anharmonicity of the repulsive interaction potential, other potential-related properties are far less well understood. For example, we find, from a sparse set of preliminary simulations for EAM systems, that there is a qualitative relationship between the plasticity threshold and the unstable stacking fault energy; that is, both appear to be lower than for the corresponding effective pair potential. There is a need, as we have done for pair-potential solids, to quantify this relationship more thoroughly. Third, because both elastic wave speed and plasticity depend on crystal orientation, it will be necessary to probe fcc perfect-crystal shock response under ⟨110⟩ and ⟨111⟩ propagation directions, in addition to ⟨100⟩ already studied. Shock behavior in other crystal lattices and for other kinds of interactions must also be explored. Finally, it will be necessary to expand our repertoire of defects for large-scale NEMD shock-wave simulations, especially to include nanocrystalline samples, where effects of both elastic and plastic anisotropy can be probed.

REFERENCES AND NOTES

1. B. L. Holian and G. K. Straub, *Phys. Rev. Lett.* **43**, 1598 (1979).
2. G. K. Straub, B. L. Holian, R. E. Swanson, *Bull. Am. Phys. Soc.* **25**, 549 (1980).
3. V. Y. Klimenko and A. N. Dremin, in *Detonatsiya, Chernogolovka*, O. N. Breusov *et al.*, Eds. (Akademii Nauk, Moscow, 1978), p. 79.
4. B. L. Holian, W. G. Hoover, B. Moran, G. K. Straub, *Phys. Rev. A* **22**, 2498 (1980).
5. W. G. Hoover, *Phys. Rev. Lett.* **42**, 1531 (1979).
6. B. L. Holian, *Phys. Rev. A* **37**, 2562 (1988).
7. ———, *Shock Waves* **5**, 149 (1995).
8. E. B. Zaretsky, G. I. Kanel, P. A. Mogilevsky, V. E. Fortov, *High Temp. Phys.* **29**, 1002 (1991).
9. M. A. Mogilevsky, in *Shock Waves and High Strain Rate Phenomena in Metals*, L. E. Murr and M. A. Meyers, Eds. (Plenum, New York, 1981), p. 531.
10. S. J. Zhou, D. M. Beazley, P. S. Lomdahl, B. L. Holian, *Phys. Rev. Lett.* **78**, 479 (1997); S. J. Zhou, D. M. Beazley, P. S. Lomdahl, A. F. Voter, B. L. Holian, in *Ninth International Conference on Fracture*, B. L. Karihaloo *et al.*, Eds. (Pergamon, Sydney, 1997), p. 3085.
11. The SPaSM ("Scalable Parallel Short-Range Molecular Dynamics") code is described in: P. S. Lomdahl, P. Tamayo, N. Grønbech-Jensen, D. M. Beazley, *Proceedings of Supercomputing 93*, IEEE Computer Society Press, 520 (1993); D. M. Beazley and P. S. Lomdahl, *Parallel Comput.* **20** 173 (1994); D. M. Beazley and P. S. Lomdahl, *Comput. Phys.* **11**, 230 (1997).
12. C. S. Smith, *Trans. Metall. Soc. AIME* **212**, 574 (1958); J. W. Taylor, *J. Appl. Phys.* **36**, 3146 (1965); J. J. Gilman, *Appl. Mech. Rev.* **31**, 767 (1968).
13. B. L. Holian and R. Ravelo, *Phys. Rev. B* **51**, 11275 (1995).
14. B. L. Holian *et al.*, *Phys. Rev. A* **43**, 2655 (1991).
15. R. L. Blumberg Selinger, private communication.
16. E. Zaretsky, *Acta Metall. Mater.* **43**, 193 (1995); M. A. Meyers, *Scripta Metall.* **12**, 21 (1978).
17. J. N. Johnson and L. M. Barker, *J. Appl. Phys.* **40**, 4321 (1969); J. R. Asay and L. C. Chhabildas, in (*12*), p. 417; J. Lipkin and J. R. Asay, *J. Appl. Phys.* **48**, 692 (1985); J. W. Swegle and D. E. Grady, *ibid.* **58**, 692 (1985); D. Tonks, in *Shock Waves in Condensed Matter*, S. C. Schmidt and N. C. Holmes, Eds. (North-Holland, Amsterdam, 1987), p. 231.
18. C. T. White, D. H. Robertson, M. L. Elert, D. W. Brenner, in *Microscopic Simulations of Complex Hydrodynamic Phenomena*, M. Mareschal and B. L. Holian, Eds. (Plenum, New York, 1992), p. 111; D. W. Brenner, D. H. Robertson, M. L. Elert, C. T. White, *Phys. Rev. Lett.* **70**, 2174 (1993).
19. A. B. Belonoshko, *Science* **275**, 955 (1997).

20. It is a distinct pleasure to thank our colleagues J. Hammerberg, D. Beazley, S. Zhou, and R. Ravelo. We also benefited from discussions with A. Belonoshko, E. Zaretsky, P. Makarov, R. Selinger, R. Mikulla, T. Germann, W. Hoover, C. White, and R. Thomson. The work at Los Alamos was encouraged by S. Younger and supported by the U.S. Department of Energy.

24 February 1998; accepted 12 May 1998